Inorganic Chemistry

Article

pubs.acs.org/IC

Alkali Metal Ion Templated Transition Metal Formate Framework Materials: Synthesis, Crystal Structures, Ion Migration, and Magnetism

Espen Eikeland,[†] Nina Lock,[‡] Mette Filsø,[†] Marian Stingaciu,[†] Yanbin Shen,[†,‡] Jacob Overgaard,[†] and Bo Brummerstedt Iversen*[,†]

[†]Center for Materials Crystallography, Department of Chemistry and iNANO and [‡]Interdisciplinary Nanoscience Center, Aarhus University, DK-8000 Aarhus C, Denmark

Supporting Information

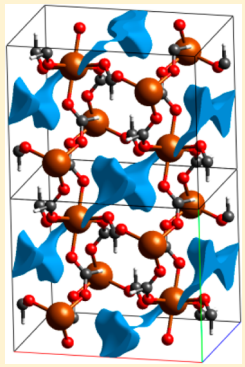

ABSTRACT: Four transition metal formate coordination polymers with anionic frameworks, namely, $Na[Mn(HCOO)_3]$, $K[Mn(HCOO)_3]$, $Na_2[Cu_3(HCOO)_8]$, and $K_2[Cu_5(HCOO)_{12}]$, were synthesized using a mild solution chemistry approach. Multitemperature single-crystal (100−300 K) and powder X-ray diffraction studies of the compounds reveal structures of large diversity ranging from cubic chiral Na−Mn formate to triclinic Na−Cu formate. The structural variety is caused by the nature of the transition metals, the alkali metal ion templation, and the versatility of the formate group, which offers metal−metal coordination through three different O−C−O bridging modes (*syn*−*syn*, *syn*−*anti*, *anti*−*anti*) in addition to metal−metal bridging via a single oxygen atom. The two manganese(II) compounds contain mononuclear, octahedrally coordinated moieties, but the three-dimensional connectivity between the manganese octahedra is very different in the two structures. The two copper frameworks, in contrast, consist of binuclear and mononuclear moieties (Na−Cu formate) and trinuclear and mononuclear moieties (K−Cu formate), respectively. Procrystal electron density analysis of the compounds indicates one-dimensional K^+-ion conductivity in K−Mn and K−Cu, and the nature of the proposed potassium ion migration is compared with results from similar analysis on known Na^+ and K^+ ion conductors. K−Mn and Na−Mn were tested as cathode materials, but this resulted in poor reversibility due to low conductivity or structural collapse. The magnetic properties of the compounds were studied by vibrating sample magnetometric measurements, and their thermal stabilities were determined by thermogravimetric analysis and differential thermal analysis. Despite structural differences, the metal formates that contain the same transition metal have similar magnetic properties and thermal decomposition pathways, that is, the nature of the transition metal controls the compound properties.

INTRODUCTION

Metal−organic frameworks (MOFs) constitute a rapidly growing class of hybrid materials with very promising properties and functionalities. MOFs consist of metal ions connected through organic linkers forming extended, often porous and three-dimensional (3D) structures.[1,2] These materials benefit from having characteristics from both the organic and inorganic building blocks, which open up the possibility of exotic materials with new and interesting properties. These properties include selective gas adsorption,[3] hydrogen storage,[4] catalysis,[5] luminescence,[6] magnetism,[7] and ionic conductivity. Although conventional batteries are based on inorganic electrode materials (e.g. Li-ion and metal hydride/nickel systems), MOFs represent an attractive alternative owing to their open and tunable channels allowing rapid intercalation.[8]

MOF compounds form through the reaction of a bridging ligand with a metal ion, which has more than one vacant/labile site. The most-used ligands are rigid molecules or ions containing oxygen (e.g., water, hydroxide, alkoxide, alcohol, and carboxylate) or nitrogen (e.g., amine, pyridine, azide, and azole).[7] The formate anion ($HCOO^-$) is the simplest and smallest carboxylate ligand; it can connect two metal ions via three different O−C−O bridging modes, namely, *syn*−*syn*, *syn*−*anti*, *anti*−*anti*,[9,10] as well as through a single oxygen atom. This results in large structural diversity for metal formates. In the *syn*−*anti* bridging mode the first metal−oxygen coordination is parallel to the C−H bond, while the second metal−oxygen coordination is parallel to the opposite C−O bond, Figure 1.

Numerous isotropic series of amine-templated anionic formates with the formula $[AmineH_n][M(HCOO)_3]_n$ (Ami-

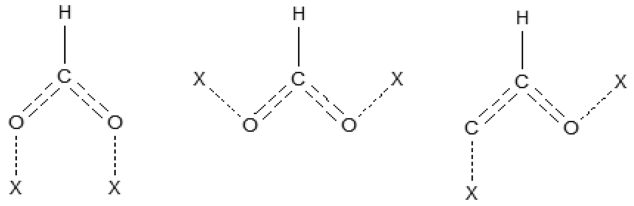

Figure 1. Different coordination modes of the formate anion. (left) *syn*−*syn*. (middle) *anti*−*anti*. (right) *syn*−*anti*.

Received: May 20, 2014
Published: September 18, 2014

   dx.doi.org/10.1021/ic501152j | *Inorg. Chem.* 2014, 53, 10178−10188

Table 1. Crystallographic Data

chemical formula	$Na[Mn(HCOO)_3]$	$K[Mn(HCOO)_3]$	$Na_2[Cu_3(HCOO)_8]$	$K_2[Cu_5(HCOO)_{12}]$
M_r/u	212.98	229.09	596.74	936.12
T/K	100	100	100	100
crystal system	cubic	monoclinic	triclinic	orthorhombic
space group	$P2_13$	$C2/c$	$P\bar{1}$	$Pbca$
a/Å	9.1286(4)	10.7818(4)	7.6153(3)	10.7430(3)
b/Å		9.0778(3)	7.7078(3)	6.8335(2)
c/Å		7.0124(3)	8.7311(3)	35.0543(9)
α/deg		90	113.058(4)	90
β/deg		94.295(1)	108.166(3)	90
γ/deg		90	98.051(3)	90
V/Å^3	760.70(6)	684.41(4)	427.42(3)	2573.4(1)
Z	4	4	1	4
P_{calc}/(g/cm^3)	1.860	2.223	2.318	2.416
F(000)	420	452	293	1836
θ_{max}, θ_{max}/deg	3.16, 34.90	2.94, 30.29	2.76, 29.23	1.16, 28.31
μ/mm^{-1}	1.77	2.514	3.834	4.496
$N_{Tot,obs}$	5386	6363	8168	29154
$N_{Uni,obs}$	1114	1020	1961	3077
N_{Obs} [I \> $2\sigma(I)$]	1007	870	1732	2627
N_{Par}	34	55	137	196
R_1, R_1 [F^2 >$2\sigma(F^2)$]	0.0361, 0.0291	0.0327, 0.0235	0.0356, 0.0281	0.0308, 0.0236
wR_2, wR_2 [F^2 >$2\sigma(F^2)$]	0.0607, 0.0580	0.0433, 0.0415	0.0658, 0.0690	0.0794, 0.0650
GOF	1.047	1.075	1.056	1.128

neH_n = $CH_3NH_3^+$, $(CH_3)_2NH_2^+$, M = Mn, Fe, Co, Ni, Cu, and Zn) have previously been studied intensively due to their promising magnetic, dielectric, porous, and optical properties.[9−12] These compounds consist of a negatively charged framework and charge stabilizing protonated amines (e.g. $CH_3NH_3^+$, $(CH_3)_2NH_2^+$). The template effect originates from the formation of hydrogen bonds between the protonated amines and the anionic framework. Changing the template cations can therefore yield a variety of different structures depending on the cation size, shape, and charge.[10]

Here we present a study on anionic formate frameworks synthesized under mild solution conditions using alkali metal cations instead of protonated amines as template and counterion. This approach was foreseen to result in considerably different templating effects as the alkali metal ions are smaller, spherical, and lack the ability to form hydrogen bonds. Moreover, the hardness/softness of the ion is changing by ascending the group. Alkali metal templated anionic formates form a new class of compounds of which few structures have been reported. One such known compound is $K[Co(HCOO)_3]$, which was reported to exhibit a transition between a chiral and an achiral polymorph.[13] We synthesized and characterized the following four anionic transition metal formates: $Na[Mn(HCOO)_3]$, $K[Mn(HCOO)_3]$, $Na_2[Cu_3(HCOO)_8]$, and $K_2[Cu_5(HCOO)_{12}]$. All structures were investigated using multitemperature single-crystal X-ray diffraction (SCXRD) and powder X-ray diffraction (PXRD). The thermal stabilities of the compounds were examined using thermogravimetric analysis (TGA), differential thermal analysis (DTA), and magnetic susceptibilities recorded from 2 to 300 K. The Na−Mn compound has previously been obtained by hydrothermal synthesis.[14] It contains octahedrally coordinated manganese(II) ions and crystallizes in the chiral spacegroup $P2_13$ and is interesting in the context of designing chiral magnets.[14−16] The compound $Na_2[Cu_3(HCOO)_8]$, which was previously prepared by evaporation synthesis, has a structure containing linked binuclear and mononuclear formate-copper(II) moieties.[17] In the present study a new synthesis approach is used to obtain the Na−Mn and Na−Cu compounds, and detailed information about their temperature dependent structures is reported. The K−Mn and K−Cu formates have not previously been reported, although the former is isostructural to the achiral K−Co formate compound. In the K−Cu formate a rarely seen bridging mode between trinuclear and mononuclear formate-copper(II) moieties is observed. Procrystal electron density analysis of the structures resulted in identification of one-dimensional (1D) ion-migration channels for K−Mn and K−Cu formate, making them possible candidates for K^+-ion based MOF electrode materials. K^+ batteries are important for creating large-scale storage batteries, which are made up of cheap materials. $K[Mn(HCOO)_3]$ and $Na[Mn(HCOO)_3]$ are not isostructural, but the K−Mn salt also has a structure containing Mn octahedra linked in three dimensions by formate bridges. In Na−Mn formate the octahedra are linked in a triangle conformation, leading to spin frustration,[14] whereas the octahedra in K−Mn formate are linked in a skewed square confirmation without spin frustration. Despite this difference, K−Mn formate shows a single sharp antiferromagnetic-to-paramagnetic transition at 3.6 K resembling the reported magnetic phase transition in Na−Mn formate at 40 K.

EXPERIMENTIAL SECTION

Synthesis. Single crystals of $Na[Mn(HCOO)_3]$, $K[Mn(HCOO)_3]$, $Na_2[Cu_3(HCOO)_8]$, and $K_2[Cu_5(HCOO)_{12}]$ were obtained in high yields by using a synthesis procedure similar to Duan et al.[13] in which $K[Co(HCOO)_3]$ single crystals were produced. It is a mild solution chemistry approach, with all products synthesized at ambient temperature, using simple metal salts and methanol as a non-coordinationg solvent, yielding phase-pure products in one step. In our syntheses, cobalt was replaced with copper and manganese, and sodium and potassium were used as template ions.

dx.doi.org/10.1021/ic501152j | Inorg. Chem. 2014, 53, 10178−10188

Table 2. Selected Bond Distances at 100 K (Å)

				$Na[Mn(HCOO)_3]$					
Mn−O1	2.186(2)	Mn−O2	2.361(3)						
Na−O2	2.330(3)	Na−O1	2.361(3)						
				$K[Mn(HCOO)_3]$					
Mn−O1	2.190(1)	Mn−O2	2.177(1)	Mn−O3	2.173(1)				
K−O1a	2.834(1)	K−O1b	2.859(1)	K−O2	2.834(1)	K−O3	2.751(1)		
				$Na_2[Cu_3(HCOO)_8]$					
Cu1−O1	1.983(1)	Cu1−O2	1.938(1)	Cu1−O3	2.456(1)	Cu2−O3	1.969(1)		
Cu2−O4	1.974(1)	Cu2−O5	2.110(1)	Cu2−O6	1.987(1)	Cu2−O7	1.960(1)	Cu2−Cu2	2.615(1)
				$K_2[Cu_5(HCOO)_{12}]$					
Cu1−O1	1.984(1)	Cu1−O2	1.943(2)	Cu1−O3	1.956(2)	Cu1−O4	2.236(2)	Cu1−O5	1.988(1)
Cu2−O7	2.281(2)	Cu2−O8	1.972(2)	Cu2−O9	1.957(2)	Cu2−O10	1.960(2)	Cu2−O11	1.966(2)
Cu3−O4	2.319(2)	Cu3−O5	1.981(1)	Cu3−O6	1.953(2)				

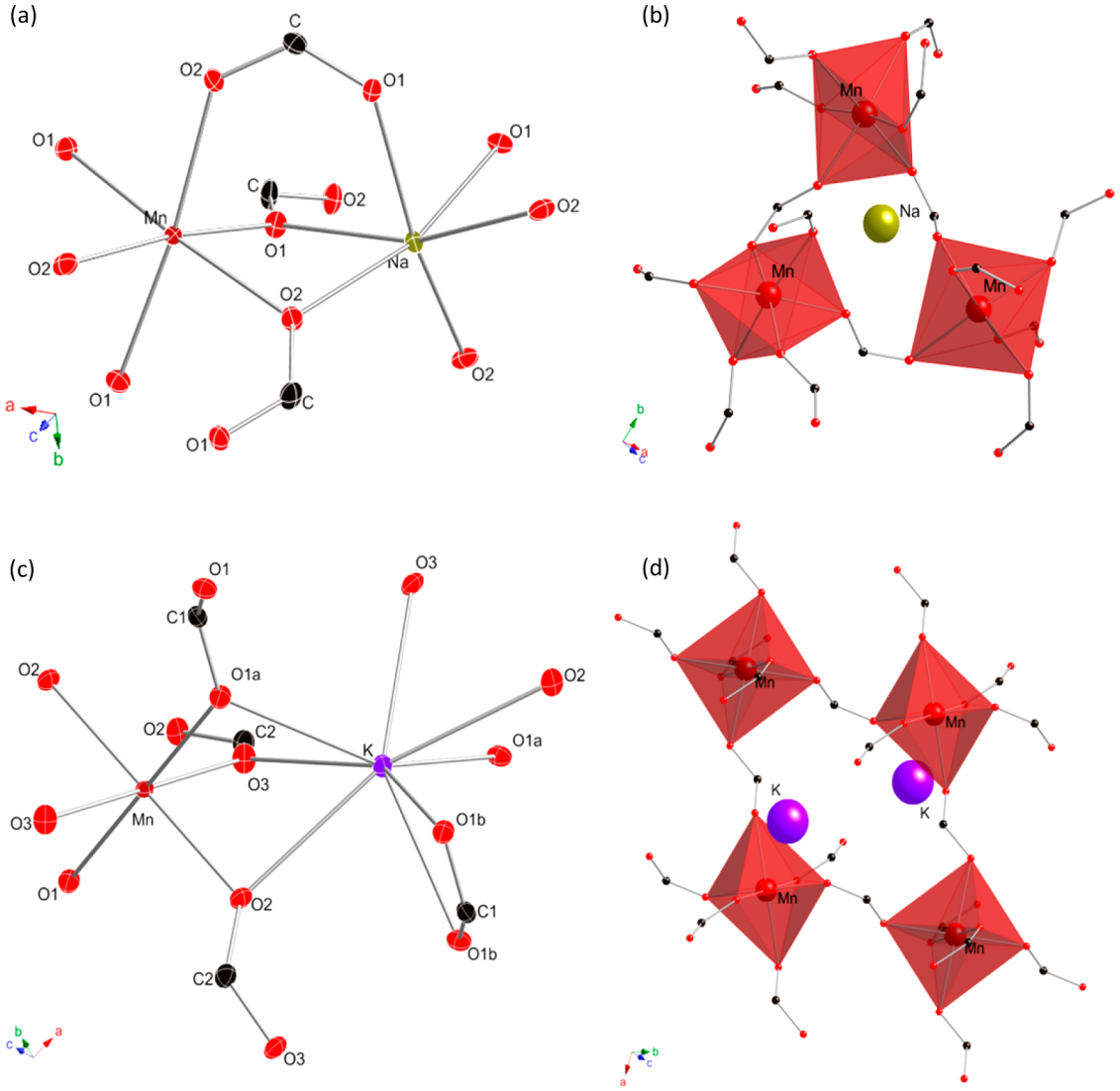

Figure 2. (a) Structure of $Na[Mn(HCOO)_3]$ with thermal ellipsoids at the 50% level and atom labels. (b) 3D connectivity of Mn octahedra in Na−Mn formate. (c) Structure of $K[Mn(HCOO)_3]$ with thermal ellipsoids at the 50% level and atom labels. (d) 3D connectivity of Mn octahedra in K−Mn formate. H atoms were omitted for clarity.

All reactants, namely, $MnCl_2{\cdot}4H_2O$, $CuCl_2{\cdot}2H_2O$, HCOONa, HCOOK, and HCOOH, are commercially available and were used without further purification. A 25 mL aliquot of 0.025 M $MCl_2{\cdot}nH_2O$ (M = Mn(II), Cu(II)) methanol solution was added to a 25 mL methanol solution of 0.20 M HCOOX (X = Na, K) and 0.53 M HCOOH. The mixture was kept at room temperature for several days, until a crystalline product had formed. The mixture was then filtrated and washed with methanol, and the crystals were dried in air for 24 h at room temperature. Identical synthesis using the 3d divalent transition metal ions Fe(II), Ni(II), Co(II), and Zn(II) were carried out, but besides the previously reported $K[Co(HCOO)_3]$[12] no anionic formate single crystals or powders were formed. The solution

dx.doi.org/10.1021/ic501152j | Inorg. Chem. 2014, 53, 10178−10188

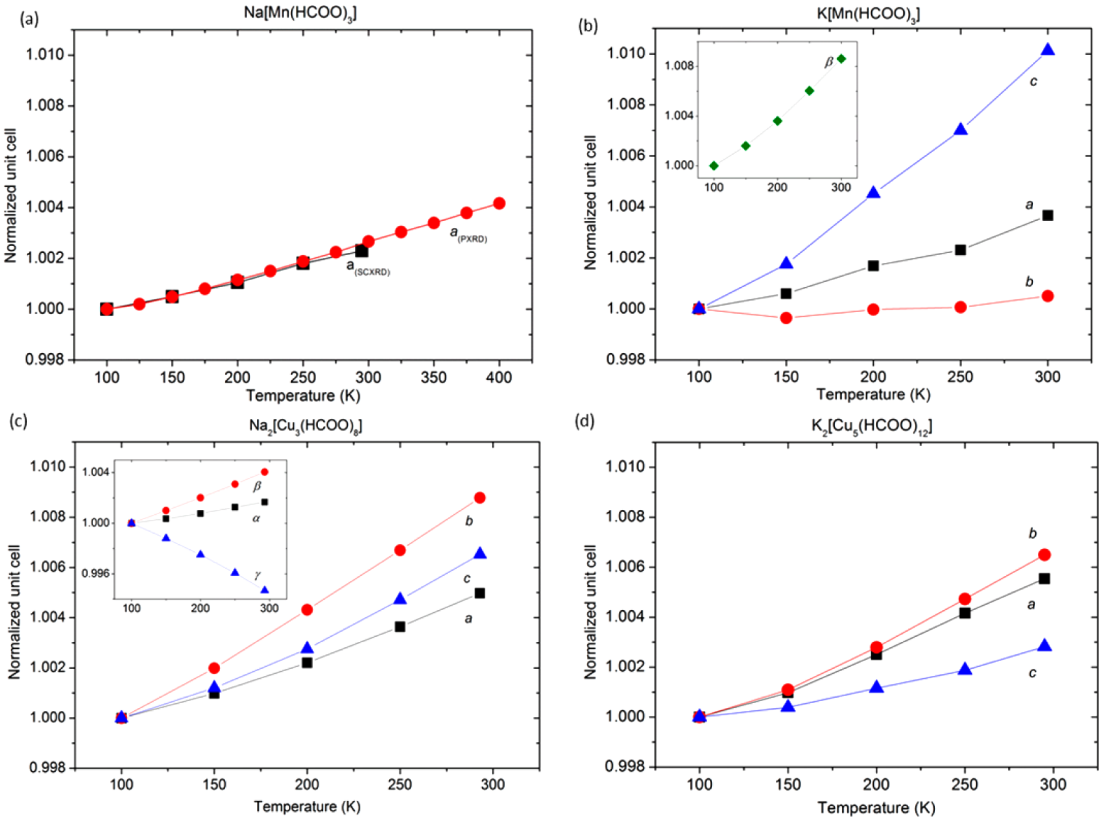

Figure 3. Normalized unit cell parameters from 100 to 300 K for (a) Na−Mn formate, (b) K−Mn formate, (c) Na−Cu formate and (d) K−Cu formate. The insets display the normalized changes in unit cell angles for nonorthogonal crystals.

containing Fe(II) transition metal ions turned brown right after the mixing indicating a reaction, while no reaction was observed in the solution containing Ni(II) or Zn(II) metal ions.

X-ray Diffraction. An in-house Rigaku SmartLab powder diffractometer was used to check the phase purity of all samples (see Supporting Information for details) at room temperature using Cu radiation (λ = 1.54 Å), parallel beam optics, and a D/teX Ultra 1D detector. The structures of $Na[Mn(HCOO)_3]$, $K[Mn(HCOO)_3]$, $Na_2[Cu_3(HCOO)_8]$, and $K_2[Cu_5(HCOO)_{12}]$ single crystals were studied using multitemperature SCXRD. The SCXRD measurements were carried out using the in-house diffractometers APEX2 from Bruker and SuperNova from Agilent Technologies, which both use Mo Kα radiation (λ = 0.710 73 Å). The temperature was controlled by a nitrogen cryostat from Oxford Cryosystems, and the diffracted intensities were collected on a CCD detector. Data from the APEX2 were integrated using SAINT+[18] and absorption-corrected in SADABS,[19] while data from the SuperNova were integrated and absorption-corrected using CrysAlisPro.[20] The structural solution and refinement were carried out in SHELX-97[21] using the WinGX GUI and Olex2.[22,23] The atomic displacement parameters (ADPs) for all atoms except hydrogen were described using an anisotropic model. In Table 1 crystallographic details and refinement residuals are listed.

Multitemperature PXRD data (100−400 K) for $Na[Mn(HCOO)_3]$ were obtained at the BL44-B2 beamline at the synchrotron facility Spring-8 in Japan using a wavelength of 0.49 Å. A Debye−Scherrer camera including an image plate setup was used for the measurements, and a cold nitrogen stream was used to control the temperature.[24] Data were integrated with software available at SPring-8, and Rietveld refinements were carried out using the FullProf program suite.[25]

Void Space and Ion Migration Analysis. The program CrystalExplorer 3.0 was used for the ion-migration pathway and void space analysis.[26] For comparison with the present structures, crystallographic information files (CIFs) for reference materials were retrieved from the Inorganic Crystal Structure Database (ICSD).[27]

Magnetic Susceptibility. The temperature-dependent magnetic susceptibility was obtained for polycrystalline samples of $Na[Mn(HCOO)_3]$, $K[Mn(HCOO)_3]$, $Na_2[Cu_3(HCOO)_8]$, and $K_2[Cu_5(HCOO)_{12}]$ using a Physical Properties Measurements System (PPMS) equipped with a vibrating sample magnetometer (VSM). Data for Na−Mn formate and K−Mn formate samples were collected in the temperature range of 2−300 K using an external applied magnetic field of 100 Oe, while for the Na−Cu formate sample a 500 Oe magnetic field was used. For the K−Cu formate sample the measurements were done in the temperature range of 12−300 K in a 1000 Oe field. An additional field-cooled (FC) measurement was also performed for the K−Mn formate sample at the same magnetic field and temperature interval. All measured susceptibilities were corrected for diamagnetic contributions using Pascal's method using the following values: $\chi_{Di,Na+} = -6.8 \times 10^{-6}$ emu mol^{-1}, $\chi_{Di,K+} = -14.9 \times 10^{-6}$ emu mol^{-1}, $\chi_{Di,Mn2+} = -14 \times 10^{-6}$ emu mol^{-1}, $\chi_{Di,Cu2+} = -11 \times 10^{-6}$ emu mol^{-1}, $\chi_{Di,HCOO-} = -17 \times 10^{-6}$ emu mol^{-1}.[28]

Thermal Analysis. The thermal stabilities of $K[Mn(HCOO)_3]$, $Na[Mn(HCOO)_3]$, $K_2[Cu_5(HCOO)_{12}]$, and $Na_2[Cu_3(HCOO)_8]$ were studied using a STA 449 C Jupiter TGA/DTA Instruments. All samples were ground, and data were collected from room temperature to 500 °C by increasing the temperature 10 °C/min in a nitrogen flow.

RESULTS AND DISCUSSION

Crystal Structures. Crystallographic data in the following sections refer to data at 100 K unless stated otherwise, and Tables 1 and 2 sum up the data. The structure of $Na[Mn(HCOO)_3]$ is shown in Figure 2a and b. The compound crystallizes in the chiral cubic space group $P2_13$, with Mn(II) and Na(I) metal ions located on the 3-fold rotation axes along the unit cell body diagonals. Mn(II) and Na(I) each coordinate to six formate groups in a distorted octahedral environment. The manganese and sodium octahedra

dx.doi.org/10.1021/ic501152j | Inorg. Chem. 2014, 53, 10178−10188

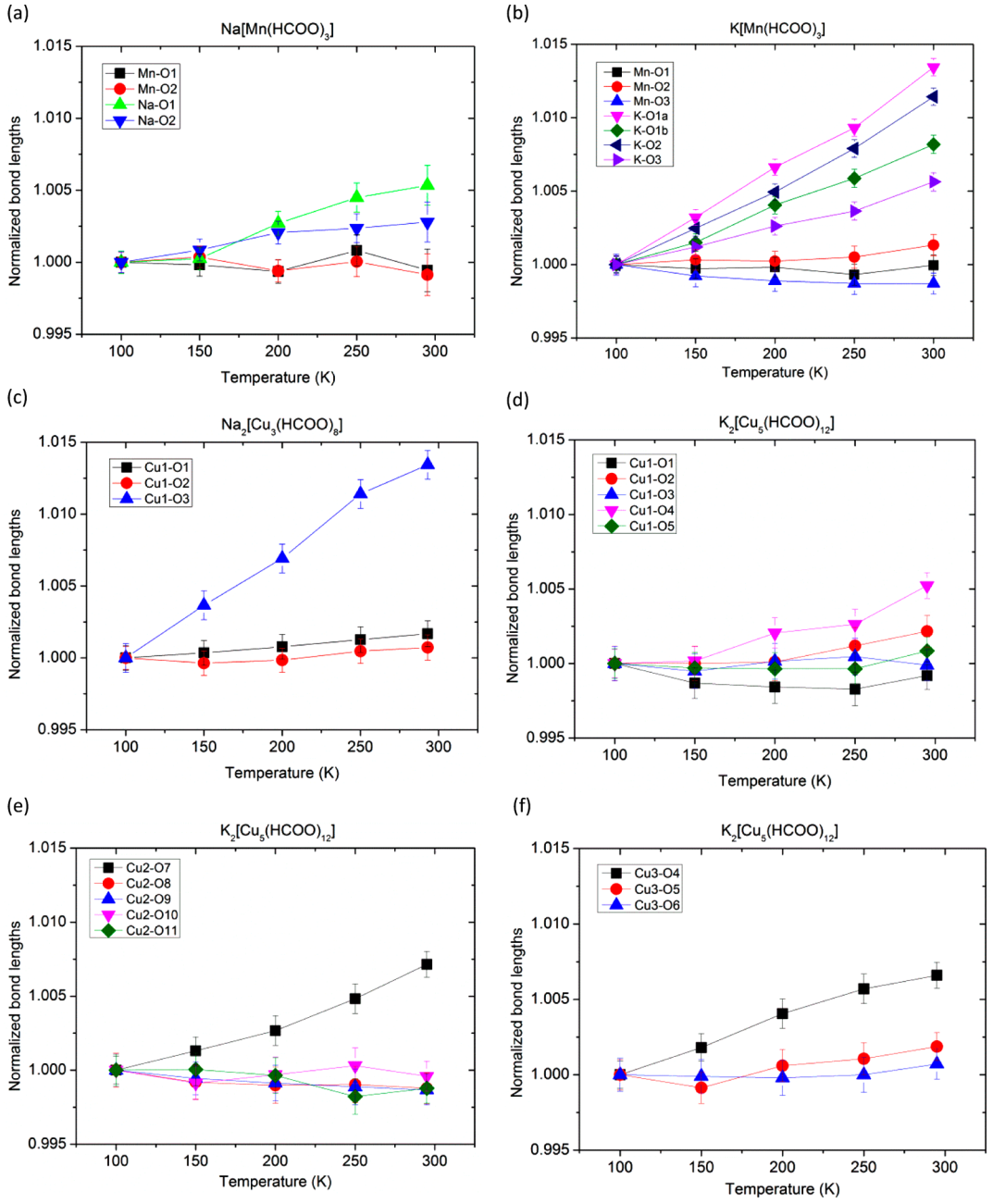

Figure 4. Changes in M−O bond lengths from 100 to 300 K for (a) Na−Mn formate, (b) K−Mn formate, (c) Na−Cu formate, and (d−f) K−Cu formate.

are edge-sharing through the O1−O2 edge and are further connected through an O2−C−O1 formate bridge. Each Mn(II) octahedron coordinates to six other Mn(II) centers through *syn*−*anti* formate bridges. Furthermore, three Mn(II) octahedra are connected in a triangle conformation as illustrated in Figure 2b. Such configurations can in some cases lead to spin frustration.[14,29]

The multitemperature SCXRD data reveal a linearly increasing cell parameter from 9.1286(4) Å to 9.1496(5) Å in the temperature range of 100−295 K. Refinements of synchrotron PXRD data show a linear increase from 9.14148(2) Å to 9.17959(5) Å in the temperature range of 100−400 K. Comparison of the two methods shows that the expansion rates d*a*/d*T* are nearly identical (Figure 3a), but that there is a slight offset in the absolute value of the cell parameter. The unit cell volume changes 0.69% in the temperature interval of 100−295 K (760.70(6)−765.96(7) Å^3) based on the SCXRD data. Furthermore, the SCXRD data shows that the Mn−O bond lengths are constant within the covered temperature range while the Na−O distances increase (Figure 4a). The isotropic ADPs for Mn and Na, namely, $U_{iso,Mn}$ and $U_{iso,Na}$, increase nearly linearly in the temperature range of 100−295 K (SCXRD data) with comparable values. $U_{iso,Mn}$ increase from 0.0077(1) Å^2 to 0.0197(2) Å^2, while $U_{iso,Na}$ increase from 0.0084(2) Å^2 to 0.0222 (5) Å^2.

The structure of K[Mn(HCOO)$_3$] is shown in Figure 2c,d. This compound crystallizes in the monoclinic space group *C*2/*c*, with the Mn atom positioned at an inversion center in a distorted octahedral environment. These Mn(II) octahedra coordinate to six other Mn(II) octahedra through 4 *syn*−*anti*

dx.doi.org/10.1021/ic501152j | *Inorg. Chem.* 2014, 53, 10178−10188

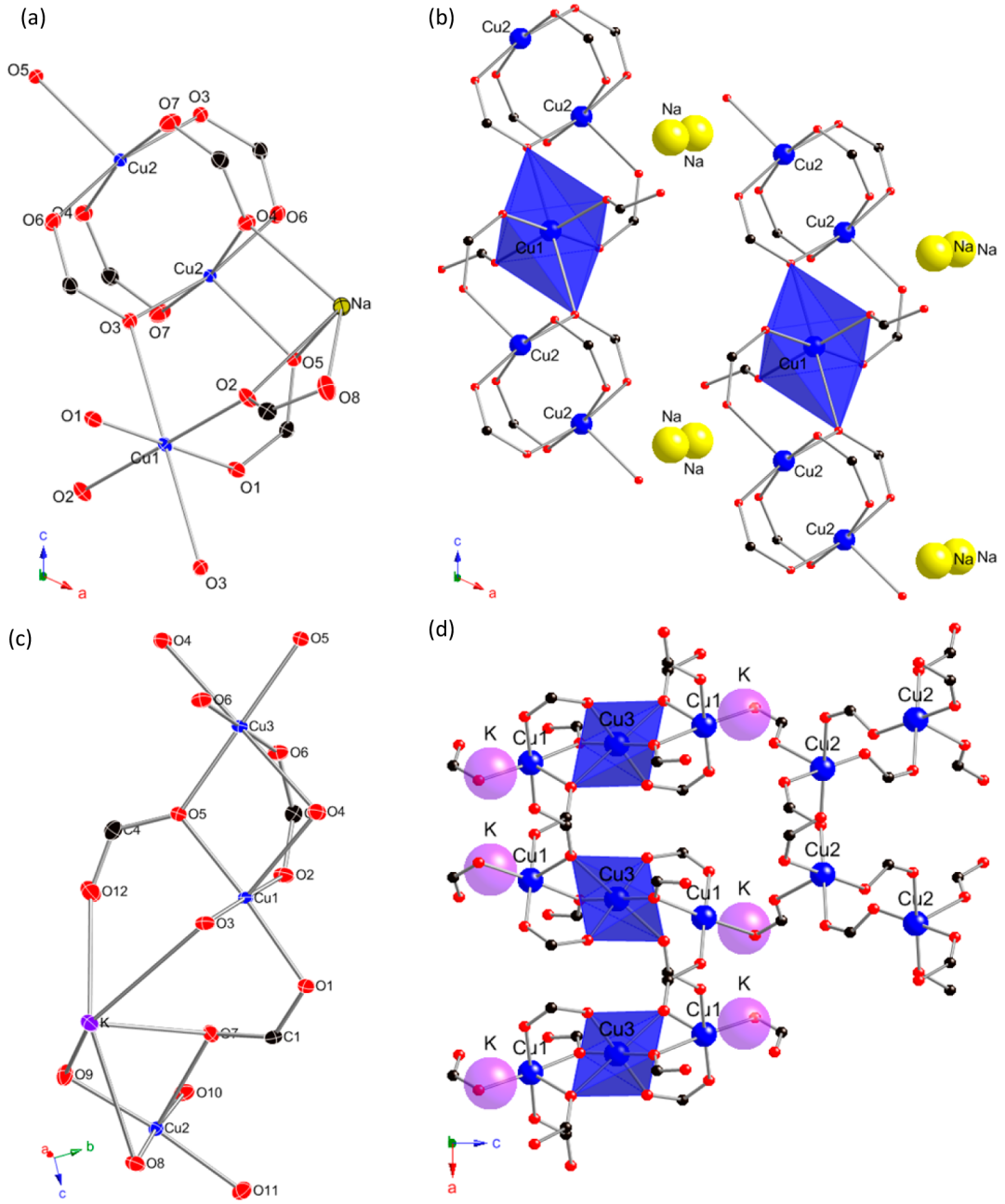

Figure 5. (a) The structure of $Na_2[Cu_3(HCOO)_8]$ with thermal ellipsoids at the 50% level and atom labels. (b) The coordination of Cu in $Na_2[Cu_3(HCOO)_8]$ illustrating the mononuclear and binuclear paddlewheel copper(II) moieties. (c) The structure of $K_2[Cu_5(HCOO)_{12}]$ with thermal ellipsoids at the 50% level and atom labels. (d) The coordination of Cu in $K_2[Cu_5(HCOO)_{12}]$ illustrating the trinuclear and mononuclear copper(II) moieties. H atoms were omitted for clarity.

and 2 *anti*−*anti* formate bridges. Compared with Na−Mn formate, four adjacent Mn octahedra in K−Mn formate are connected to form a skewed square conformation illustrated in Figure 2d. This differs from the triangular conformation in Na−Mn, and it does not lead to similar spin frustration. Each Mn atom is linked to two K atoms through three oxygen atoms (O1, O2, O3) from three different formate groups. The potassium ion is located at a 2-fold rotation axis parallel to the *b*-axis and coordinates to eight oxygen atoms with four different bond lengths.

Normalized unit cell parameters for $K[Mn(HCOO)_3]$ at different temperatures are plotted in Figure 3b. The unit cell expands at different rates along the different cell axes. The shortest cell axis (c = 7.0124(3)) changes the most (1.010(5)%), while the length of the unique b axis is almost unchanged (0.051(4)%) in the studied temperature range. The unit cell volume changes 1.30(1)% in the measured temperature interval (684.41(5)−693.42(3) Å^3), which is almost twice the amount the Na−Mn unit cell expands in the same temperature interval (0.69%). The Mn−O and K−O bond distances are plotted in Figure 4b as a function of temperature, and the Mn−O bond distances are largely constant with temperature as were the corresponding distances in Na−Mn formate (Figure 4a). The coordination distances between potassium and the surrounding oxygen atoms increase linearly (~0.5−1.3%) as the temperature is raised, and the changes are

dx.doi.org/10.1021/ic501152j | *Inorg. Chem.* 2014, 53, 10178−10188

much larger than for the relative Na−O distance changes in the Na−Mn formate (Figure 4a).

The U_{iso} values for Mn and K show linear increases for $U_{iso,Mn}$ and $U_{iso,K}$ in the covered temperature range (100 to 300 K). The $U_{iso,Mn}$ values are similar for the $K[Mn(HCOO)_3]$ (0.0076(1) Å^2 to 0.0177(1) Å^2) and $Na[Mn(HCOO)_3]$ structures, while the $U_{iso,K}$ values (0.0109(1) Å^2 to 0.0291(1) Å^2) are considerably larger than the $U_{iso,Na}$ values in the studied temperature range. In summary, the larger change in the unit cell volume, alkali metal−oxygen distance and the isotropic ADPs for the alkali metal ion in $K[Mn(HCOO)_3]$ in comparison with Na[Mn(HCOO)3] point to a more flexible and looser bound potassium than sodium ion. This may be explained by the fact that the potassium ion is larger and hence softer.

The structure of $Na_2[Cu_3(HCOO)_8]$ is shown in Figure 5a,b. The compound crystallizes in the triclinic space group $P\bar{1}$, and it contains dinuclear copper(II)-formate complexes, where two equivalent copper(II) sites (Cu2) are *syn*−*syn* linked by four formate bridges. This geometry is also known as the paddlewheel structure type.[30] An inversion center is located between the two linked copper atoms (Cu2). The Cu2 atoms also coordinate to a fifth oxygen atom (O5) resulting in a 4 + 1 environment.[17] Furthermore, the structure contains a mononuclear Cu(II) site (Cu1) located on an inversion center, and this Cu atom exhibits a strong Jahn−Teller distortion. The four equatorial O atoms (d_{Cu1-O1} = 1.984(1) Å, d_{Cu1-O2} = 1.938(1) Å) are positioned closer to the copper center than the two O3 atoms (d_{Cu1-O3} = 2.457(2) Å), which in turn are a part of the square paddlewheel structure.[31] The result is an infinite chain of alternating dinuclear and mononuclear moieties coupled together by *syn*−*syn* formate bridges. This coordination type is rarely seen in Cu(II) formate complexes.[17] Each Na coordinates to seven oxygen atoms with Na−O distances varying from 2.3 Å to 2.7 Å.

The unit cell of Na−Cu formate expands along all three axes in the measured temperature interval with an approximately linear increase (Figure 3c). The unit cell angles α and β increase linearly from 113.023(4) to 113.213(5)° and from 108.171(4) to 108.610(4)°, respectively, while γ decreases from 98.073(3)° to 97.552(4)°. Thus, the unit cell volume increases in the whole temperature range from 427.79(3) to 435.47(3) Å^3 (1.76(1)%) The changes of the Cu1−O bond distances with temperature are displayed in Figure 4c. The coordination distances to the four equatorial oxygen atoms (O1 and O2) are almost constant within uncertainties, while the change in Cu1−O3 bond distance is much larger with a 1.3(1)% expansion. This means that the Jahn−Teller distortion gets more pronounced at increasing temperatures. The Cu2−O bond distances are all constant within uncertainties (~2.0 Å), while the Cu2−Cu2 distance increases linearly from 2.6154(4) to 2.6227(4) Å corresponding to a growth of 0.28(2)% (see Supporting Information). The large expansion of the Cu1−O3 bond distance compared with all the other Cu−O bonds, including the Cu2−O3 distance, could indicate that the coordination of oxygen around Cu1 may be more square planar than octahedral in character that is, the Cu1−O3 bond order is low. The isotropic ADPs for the two Cu atoms and Na show a linear increase from 100 to 293 K. The U_{iso} values for the two Cu atoms are almost identical (~0.008 Å^2 at 100 K to 0.020 Å^2 at 293 K) and similar to the values for Mn in the $K[Mn(HCOO)_3]$ and $Na[Mn(HCOO)_3]$ structures. Na has somewhat higher U_{iso} values (0.0109(2) to 0.0249(2) Å^2) compared with Cu, but also compared with the U_{iso} values for Na in $Na[Mn(HCOO)_3]$.

The structure of $K_2[Cu_5(HCOO)_{12}]$ is displayed in Figure 5c,d. The compound crystallizes in the orthorhombic space group *Pbca* with an elongated unit cell. The structure contains three different Cu(II) sites, and copper appears in both a trinuclear copper chain (Cu1 and Cu3) geometry and as mononuclear copper (Cu2). Cu3 is located on an inversion site, and it is octahedrally coordinated to six oxygen atoms. The Jahn−Teller effect is observed, with the Cu3−O4 distance (2.32 Å) considerably longer than the two other Cu−O distances (~2.0 Å). Cu3 is linked to two Cu1 sites, each through two oxygen atoms (O4 and O5) and a *syn*−*syn* formate bridge. The Cu1···Cu3 distance is 3.177(1) Å, which is considerably longer than the paddle-wheel Cu2···Cu2 distance in the Na−Cu formate of 2.615(1) Å. Cu1 is coordinated in a 4 + 1 environment with the five coordinating oxygen atoms belonging to different formate groups. The bond distance from Cu1 to the four equatorial oxygen atoms is ~2.0 Å, while the last oxygen atom (O4) is found at a distance of 2.236(2) Å. The mononuclear copper site consists of Cu2, which also has a 4 + 1 environment build from five different formate bridges. Four of these formate bridges link to two other Cu2 sites (*syn*−*anti*), and one links to the trinuclear copper chain (*syn*−*anti*). Potassium coordinates to 10 oxygen atoms at distances between 2.7 Å and 3.4 Å.

The unit cell lengths between 100 and 300 K are shown in Figure 3d. The two shorter cell axes, *a* and *b*, have larger relative thermal expansion (~0.6%) compared with the longer *c*-axis (~0.3%), resulting in a total unit cell volume change of 1.47(1)% (2573.42(12)−2611.82(8) Å^3). The relative changes of the Cu−O bond lengths as a function of temperature are displayed in Figure 4d−f. The equatorial Cu1−O bond distances are almost constant within uncertainties, while the remaining Cu1−O4 bonds perpendicular to the others expand 0.5(1)% in the covered temperature range (Figure 4d). For Cu2 the four equatorial oxygen distances slightly decrease as temperature is raised, however barely significantly, while the Cu2−O7 bond perpendicular to the other Cu2−O bonds increase linearly 0.7(1) % (Figure 4e). The equatorial Cu3−O5 and Cu3−O6 distances remains almost unchanged, while the Jahn−Teller shifted Cu3−O4 bond distance expand 0.7(1)% (Figure 4f). This expansion is about half of the increase in the similar Jahn−Teller distorted Cu−O3 bond in the Na−Cu formate structure. For all three Cu sites in $K_2[Cu_5(HCOO)_{12}]$ the equatorial oxygen distances change less compared with the axial Cu−O distances with increasing temperature. The isotropic ADPs for the three copper atoms and for potassium increase linearly from 100 to 295 K. The Cu atoms all have very similar isotropic ADPs (~0.009 Å^2 at 100 K to 0.020 Å^2 at 293 K), also when compared to the Cu sites in the Na−Cu formate structure. In the case of potassium it has similar U_{iso} values in the K−Cu (0.0119(2) Å^2 to 0.0295(2) Å^2) and the K−Mn formate structures.

Void Space Analysis. Procrystal electron density analysis is used determine the void space and possible ion-migration pathways within the structures.[31,32] The procrystal electron density ρ_{pro} is defined as the sum of spherical atomic electron densities in the unit cell. From ρ_{pro}, it is possible to draw different iso-density surfaces, each iso-density value partitioning the unit cell into regions of higher and lower ρ_{pro} values. In this way Turner et al. showed that an isovalue of 0.0003 atomic units (au) is a sensible value for probing porosity and

dx.doi.org/10.1021/ic501152j | Inorg. Chem. 2014, 53, 10178−10188

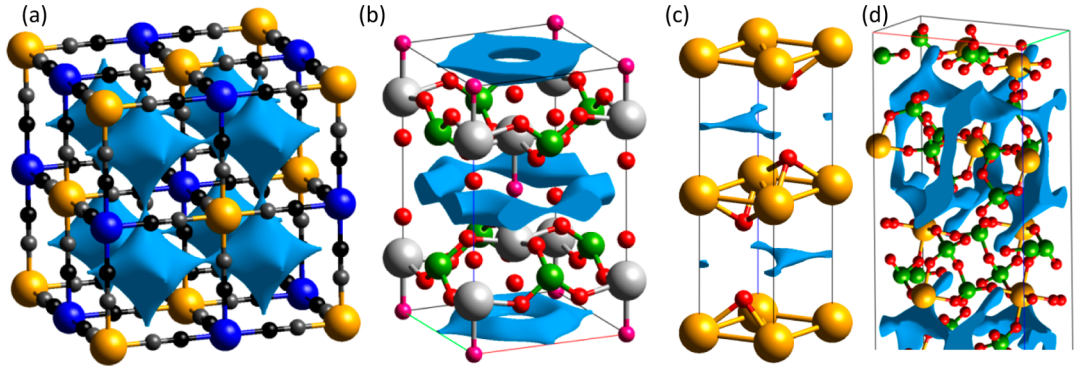

Figure 6. (a) 3D K^+ ion migration channels in copper hexacyanoferrate ($CuK[(CN)_6Fe]$) at an isovalue of 0.0007 au. Prussian blue and copper hexacyanoferrate are isostructural with Fe replacing the Cu position. (b,c,d) 2D Na^+ ion migration channels in $Na_{1.5}VPO_5F_{0.5}$ (b), $Na_{3/4}[Fe_{2/3}Mn_{1/3}]O_2$ (c), and α-$Na_7Fe_3(P_2O_7)_4$ (d) at isovalues of 0.0014, 0.0016, and 0.0007 au, respectively. For $Na_{3/4}[Fe_{2/3}Mn_{1/3}]O_2$ only Fe atoms are displayed although 1/3 of these positions are Mn. Cu (dark blue), Fe (orange), C (dark gray), N (black), P (green), O (red), F (pink), V(light gray), Mn (brown), and isosurfaces (light blue).

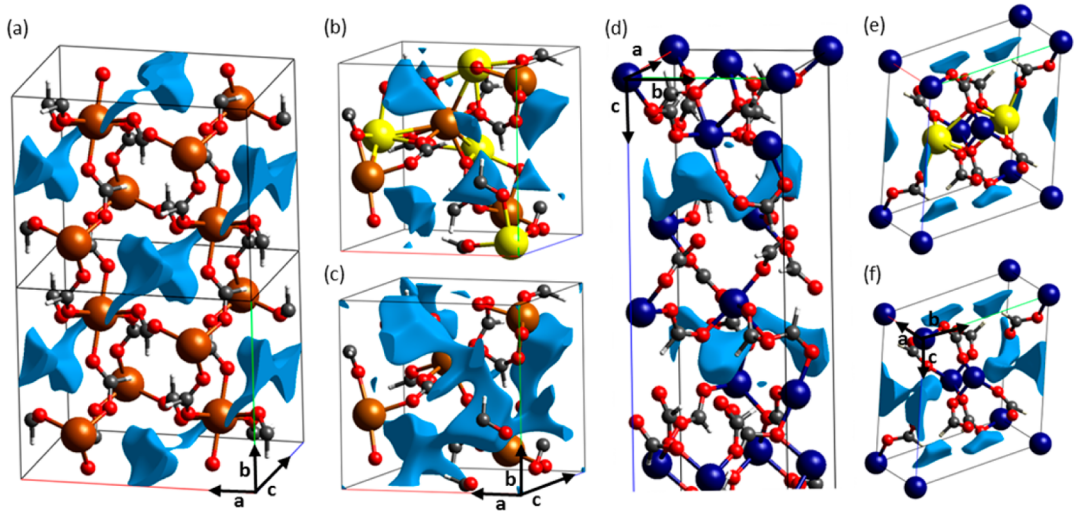

Figure 7. (a) K^+ ion-migration channels in K−Mn formate at an isovalue of 0.0007 au. (b,c) 0.0006 au isosurface of Na−Mn formate with and without Na in the structure. (d) K^+ ion-migration channels in K−Cu formate at an isovalue of 0.0005 au. (e,f) 0.0009 au isosurface in NaCu-formate with and without Na^+ in the structure. Mn (brown), Na (yellow), Cu (dark blue), C (gray), O (red), H (white), and isosurfaces (light blue).

visualizing empty space in molecular crystals.[31] An isosurface of 0.0020 au on the other hand has been established as a sensible value for a smoothed van der Waals (VdW) surface.[32]

Indication of porosity was only found in the Na−Mn formate structure where an isovalue of 0.0003 au results in very small void space regions of 2.35 Å^3 per unit cell. This void space is too small to accommodate solvent molecules but illustrates that the structure contains low electron density regions. None of the other structures (Na−Cu, K−Cu, K−Mn) contain voids at this isocontour level and must be regarded as non-porous structures. The 0.0020 au smoothed VdW surface of the structures give a void space relative to the unit cell volume of 17.9% for Na−Mn, 0.6% for K−Mn, 7.9% for Na−Cu, and 5.6% for K−Cu. Thus, in the case of Na−Mn the volume outside the VdW surface displays broad channels in three dimensions that make up 17.9% of the structure underlining the low density regions of this structure. In strong contrast K−Mn has a very densely packed structure where the 0.0020 au surface only results in a void space of 0.63% of the unit cell. The large difference in void space in the four structures reiterates that the four structures are very different, that is, that the alkali ion templating does not direct the structure formation. Furthermore, it is noteworthy that the most porous structure is least affected by temperature with respect to unit cell and interatomic distance changes. The explanation for this may be that the porous structure can accommodate larger vibrations without expanding too much upon heating.

Ion Migration Analysis. For the ion-migration pathway analysis all relevant ions (Na or K) were removed from the structure files, and two assumptions were made. First that ions migrate in the direction of lowest ρ_{pro},[33] and second that there is some upper threshold ρ_{pro} value for migration to occur. The threshold value can be evaluated empirically by comparing and analyzing structures of well-established ion-conductors. Another important quantity for battery materials is the activation energy for ion migration. In the procrystal analysis a similar quantity $\Delta\rho_{pro}$ has been defined as the difference between the isovalue for ion migration and the ρ_{pro} value at the equilibrium ion site.[33] A low $\Delta\rho_{pro}$ value indicates low activation energy for ion migration, desirable for battery materials. Thorough explanation of the validity and limitations of the ion-migration pathway analysis can be found in the work of Filso et al. where reliable Li-ion migration pathways were predicted in numerous battery materials.[33]

dx.doi.org/10.1021/ic501152j | Inorg. Chem. 2014, 53, 10178−10188

To determine a threshold value for K^+ migration the well-known Prussian blue (PB)[34] $Fe[Fe_2(CN_6)]_3$ and the newer copper hexacyanoferrate $CuK[(CN)_6Fe]$ (CuHCF) structures[8] were analyzed. Both these electrode materials have relatively open framework structures, and in that sense they resemble the K−Mn and K−Cu formate structures. In Figure 6 three-dimensional K^+-ion migration channels are revealed at an isovalue of 0.0008 au and 0.0007 au for PB and copper hexacyanoferrate, respectively, with a $\Delta\rho_{pro}$ value of 0.0006 au for both structures. To examine Na^+ ion migration we analyze the well-known Na-ion conductors $Na_{1.5}VPO_5F_{0.5}$, $Na_{3/4}[Fe_{2/3}Mn_{1/3}]O_2$, and α-$Na_7Fe_3(P_2O_7)_4$[35−37] (Figure 6). For α-$Na_7Fe_3(P_2O_7)_4$ two-dimensional (2D) ion-migration pathways were found at an isovalue of 0.0007 au, with a $\Delta\rho_{pro}$ value of 0.0005 au. For $Na_{1.5}VPO_5F_{0.5}$ and $Na_{3/4}[Fe_{2/3}Mn_{1/3}]O_2$ the 2D migration pathway is observed at 0.0014 and 0.0016 au, with corresponding $\Delta\rho_{pro}$ values of 0.0007 au and 0.0003 au, respectively. $Na_{1.5}VPO_5F_{0.5}$ and $Na_{3/4}[Fe_{2/3}Mn_{1/3}]O_2$ exhibit relatively higher isovalues for migration due to their layered structures. Interatomic interactions between layers are often weaker than in-plane interactions, and this causes layered ion conductors to expand/contract perpendicular to the planes to optimize interactions with the migration ions. This phenomenon is readily observed in Li-ion battery materials.[33]

Turning to the materials reported in the present study the ion-migration analysis reveals possible 1D K^+ ion migration in K−Mn formate and K−Cu formate. Already at an isovalue of 0.0003 au a small elongated surface is visible in the K−Mn formate structure centered on the absent K position. At 0.0007 au the individual surfaces join in straight lines to form zigzag 1D migration pathways along the direction of the *c*-axis, resulting in a $\Delta\rho_{pro}$ value of 0.0004 au, Figure 7a. The same K^+ ion migration pathway is present in the isostructural K−Co polymorph only at 0.0006 au. In K−Cu formate an isosurface centered on the K position is visible at 0.0003 au, and already at 0.0005 au 1D K^+ ion-migration pathways are observed along the *b*-axis connecting areas centered on the K position through kinks, Figure 7d. This leads to a $\Delta\rho_{pro}$ value of 0.0002 au. In the porous Na−Mn formate structure the Na position gets incorporated in the isosurface at a value of 0.0006 au, and indeed a large part of this space was already depicted in the void space analysis, Figure 7b,c. The relatively open structure of the Na−Mn material, and therefore relatively large portion of empty space, makes it impossible to predict migration pathways since the assumption that ions migrate in the direction of lowest ρ_{pro} is no longer valid. In the case of the Na−Cu formate an isovalue of 0.0005 au leads to a surface centered on the Na position along with several others centered on the sides of the unit cell. At 0.0009 au a pathway is formed combining the Na positions along the *a*-axis, but since areas with low procrystal electron density take up a large part of this pathway it is unlikely that Na will migrate in this direction. Only at an isovalue of 0.0018 au the Na position becomes included in pathways along the remaining axes. Thus, we conclude based on procrystal analysis that Na probably remains immobile.

As revealed by the void space analysis the K−Cu and K−Mn structures are denser than the Na−Mn and Na−Cu structures. Li^+ ion migration in battery materials typically is favorable in quite dense structures since in very open structures the atomic interactions are too weak to "drive" the migrating ion through the structure. For K−Cu and K−Mn the $\Delta\rho_{pro}$ values are 0.0002 and 0.0004 au, respectively. Comparing these values to the higher $\Delta\rho_{pro}$ value of 0.0006 au for PB and copper hexacyanoferrate, suggests low activation energy for K^+ ion migration in K−Mn and K−Cu. Thus, the procrystal analysis indicates that K−Mn and K−Cu could be promising K^+ ion battery materials. Also note that both materials were synthesized using very simple and mild conditions with cheap reactants. If these materials are to be used as battery materials one has to consider the possible redox chemistry that can take place during K^+ insertion or depletion. To keep the crystal neutral K^+ insertion will necessitate a reduction of the transition metal, that is, Cu^{2+} to Cu^+ or Mn^{2+} to Mn^+, whereas K^+ depletion will lead to oxidation, that is, Cu^{2+} to Cu^{3+} or Mn^{2+} to Mn^{3+}. Since Mn does not exist in the monovalent state and Cu does not exist in the trivalent state, we predict that K−Mn is suitable for K^+ depletion, whereas K−Cu possibly can have K^+ insertion. The procrystal analysis of the four anionic formates presented herein was performed on crystallographic data at 100 K. Comparing the result to an identical analysis performed at 300 K shows that the analysis is almost temperature-independent in the measured temperature range, although the calculated void space gets slightly bigger due to unit cell expansion ($\lesssim$1.1%, relative to the unit cell volume).

On the basis of redox chemistry considerations and the above procrystal analysis, Na−Mn and K−Mn formate were tested in a sodium ion battery and lithium ion battery as cathode electrode materials. The assumption being that if K^+/Na^+ is able to migrate out of the K−Mn/Na-Mn structure without causing structure collapse then Na^+ or Li^+ ions should be able to migrate into the structure again. Ground K−Mn and a lithium counter electrode were assembled in a coin cell with an open-circuit voltage of 2.75 V. The cell voltage quickly jumped to 4 V after applying a small current density of ~0.03 mAh/cm^2 indicating very high cell impedance. At higher voltage the K^+ ions could be extracted; however, a reversible plateau at similar potential could not be found on the following discharge. At 1.4 V it seems the Li^+/K^+ can be inserted back into the structure indicating low conductivity or collapse of the structure upon the K^+ extraction. Similar results from K−Mn and Na−Mn in the sodium ion battery leads to the conclusion that K^+ and Na^+ can be extracted from K−Mn and Na−Mn, respectively, but the reversibility is poor due to low conductivity or instability of the material. These problems must be overcome if Na−Mn or K−Mn formate is to be used as a cheap battery material. A more detailed description of the battery tests can be found in the Supporting Information.

Magnetic Properties. Magnetic susceptibility measurements of the $Na[Mn(HCOO)_3]$, $Na_2[Cu_3(HCOO)_8]$, and $K_2[Cu_5(HCOO)_{12}]$ compounds all showed paramagnetic behavior in the measured temperature range (see Supporting Information). However, in the case of $K[Mn(HCOO)_3]$ compound a sharp magnetic phase transition was detected at 3.6 K, as shown in Figure 8, corrected for diamagnetic contributions. Similar phase transition is observed for the isostructural $K[Co(HCOO)_3]$ compound at 2.0 K under 10 Oe.[13] The zero field cooled (ZFC) and field cooled (FC) susceptibility curves are almost identical down to the transition at 3.6 K where a splitting is observed. The sharp increase in the FC molar susceptibility below 3.6 K may be due to the appearance of a weak ferromagnetic moment because of spin canting away from a noncollinear antiferromagnetic alignment of neighboring spins.[14,29] A similar behavior has been reported for $Na[Mn(HCOO)_3]$ where a irreversibility of the ZFC−FC susceptibility curves occurred below 40 K when measured with

dx.doi.org/10.1021/ic501152j | Inorg. Chem. 2014, 53, 10178−10188

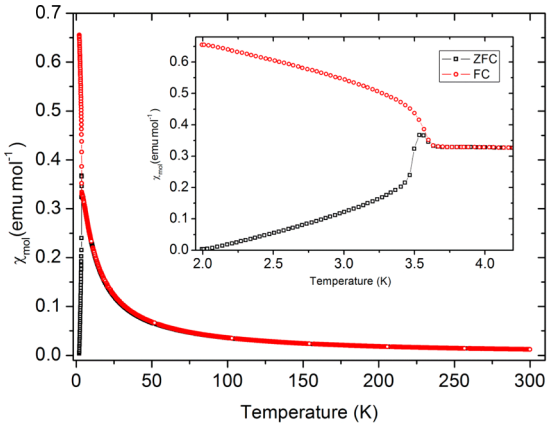

Figure 8. Magnetic susceptibility for $K[Mn(HCOO)_3]$ from 100 to 300 K at a magnetic field of 100 Oe. (inset) The magnetic transition at 3.6 K with a splitting of the field cooled (FC) and zero field cooled (ZFC) curves.

magnetic fields in the range of 20−1000 Oe.[14] The effective magnetic moment of the Mn^{2+} ions in K−Mn formate was determined to be 5.404(1) μ_B and 5.419(1) μ_B from the ZFC and the FC susceptibility curves, respectively. Susceptibility curves for the Na−Mn compound resulted in a similar effective magnetic moment ($\mu_{eff,NaMn}$ = 5.444(8) μ_B) although these values are lower than expected for uncoupled (high spin) Mn^{2+} ions (~5.9 μ_B). A more detailed magnetic study is needed to fully explain this μ_{eff} lowering, but such investigations are outside the scope of this paper.

The data collected on $Na_2[Cu_3(HCOO)_8]$ did not follow the Curie−Weiss law above 150 K. Whether this is due to slight impurities or actual sample behavior is unclear, but no impurities were observed in the PXRD data prior to the magnetic measurements. The measurements on the $K_2[Cu_5(HCOO)_{12}$ sample resulted in an effective magnetic moment of 1.810(1) μ_B, which is in agreement with high-spin Cu^{2+} ions (1.7−2.2 μ_B).[38] More information can be found in the Supporting Information.

Thermal Stabilities. From TGA and DTA measurements of the four different compounds, it is evident that the structures containing the same transition metal have very similar thermal stabilities. Na−Mn and K−Mn formate decompose at 341 and 327 °C, with significant mass losses of 39% and 32%, respectively. The decomposition in both cases consists of multiple broad steps, with the first step being endothermic. Na−Cu and K−Cu formate decompose at 147 and 144 °C, with mass losses of 48% and 44%, respectively. In contrast to the Mn-containing formates the decomposition of Na−Cu and K−Cu takes place in a very narrow temperature interval and with low onset temperatures also compared to other metal formates reported in literature, for example, $K[Co(HCOO)_3]$, where both polymorphs start to decompose at 230 °C.[10,13,39] More details about the thermal behaviors of the four materials are given in the Supporting Information.

Comparison of Structures. None of the four structures presented here are isostructural although the anionic formates with the same transition metal share structural similarities. $Na[Mn(HCOO)_3]$ and $K[Mn(HCOO)_3]$ have the same alkali metal/transition metal/formate stoichiometry and similar coordination geometries around their metal centers. However, the connectivities between the octahedral building blocks are different. In Na−Mn formate the Mn(II) octahedra arrange in triangles, while they form skewed squares in K−Mn formate. In addition, Mn(II) is coupled to Na(I) through two single atoms and one formate bridge in the Na−Mn formate structure, while Mn(II) is linked to K(I) via three single atoms only in the K−Mn formate. The effective magnetic moment of Mn(II) is similar in the two structures, but a magnetic transition is only observed in K−Mn formate. The magnetic transitions in Na−Mn formate previously described in the literature were not observed in the present study. Interestingly, the known achiral $K[Co(HCOO)_3]$ polymorph is isostructural to the monoclinic K−Mn structure, while the chiral K−Co polymorph and the chiral Na−Mn structure are highly symmetric having hexagonal and cubic crystal systems, respectively. Both $Na_2[Cu_3(HCOO)_8]$ and $K_2[Cu_5(HCOO)_{12}]$ contain multiple formate-copper(II) moieties from monomeric to trimeric. The anionic formates with the same transition metal have similar thermal decomposition pathways, indicating that the transition metal influences the thermal stability of the compounds to a greater extent than the alkali metal template/charge stabilizing ions. Anionic transition metal formates templated by amines often form isostructural series of compounds with the same amine template ion but with different transition metals. The four different structures characterized here indicate that alkali metal template ions have less impact than amines on the structure as well as the thermal stabilities. This is probably due to the alkali metal isotropic electron distribution compared with amines.

CONCLUSION

Four different metal formate complexes templated by alkali metals have been synthesized and characterized. The two new complexes contain 1D ion migration channels, while the remaining two have been synthesized in a new and simpler way resulting in purer products and higher yields. $Na[Mn(HCOO)_3]$ and $K[Mn(HCOO)_3]$ consist of a 3D network of Mn(II) octahedra forming triangle and skewed square confirmations, respectively. $Na_2[Cu_3(HCOO)_8]$ and $K_2[Cu_5(HCOO)_{12}]$ contain multiple formate-copper(II) moieties ranging from monomeric to trimeric. All structures were studied in detail by multitemperature single-crystal X-ray diffraction revealing that potassium is more loosely bonded than sodium. Moreover, it is observed that the transition metal polyhedra are nearly temperature-independent in the covered temperature range. A test of Na−Mn and K−Mn formate as battery materials was performed, but this resulted in poor reversibility due to low conductivity or decomposition. The presented mild solution synthesis can probably be generalized and used to produce new anionic metal formates with interesting structures and properties as an alternative to conventional solvothermal synthesis.

ASSOCIATED CONTENT

Supporting Information

Includes CIFs, PXRD data, magnetic measurements for all compounds, and detailed description of the electrochemical and thermal stability analysis. This material is available free of charge via the Internet at http://pubs.acs.org.

AUTHOR INFORMATION

Corresponding Author

*E-mail: bo@chem.au.dk.

Notes

The authors declare no competing financial interest.

■ ACKNOWLEDGMENTS

This work was supported by the Danish National Research Foundation (Center for Materials Crystallography, DNRF93), the Danish Research Council for Nature and Universe (Danscatt), and the Villum Foundation. RIKEN is gratefully acknowledged for beam time at beamline BL44B2 at the SPring8 synchrotron in Japan. M. Søndergaard is thanked for fruitful discussions.

■ REFERENCES

(1) James, S. L. *Chem. Soc. Rev.* **2003**, *32*, 276−288.
(2) Cheetham, A. K.; Rao, C. N. R.; Feller, R. K. *Chem. Commun.* **2006**, 4780−4795.
(3) Li, J.-R.; Kuppler, R. J.; Zhou, H.-C. *Chem. Soc. Rev.* **2009**, *38*, 1477−1504.
(4) Murray, L. J.; Dincă, M.; Long, J. R. *Chem. Soc. Rev.* **2009**, *38*, 1294−1314.
(5) O'Keeffe, M. *Chem. Soc. Rev.* **2009**, *38*, 1215−1217.
(6) Allendorf, M. D.; Bauer, C. A.; Bhakta, R. K.; Houk, R. J. T. *Chem. Soc. Rev.* **2009**, *38*, 1330−1352.
(7) Kurmoo, M. *Chem. Soc. Rev.* **2009**, *38*, 1353−1379.
(8) Wessells, C. D.; Huggins, R. A.; Cui, Y. *Nat. Commun.* **2011**, *2*, 550.
(9) Rossin, A.; Giambastiani, G.; Peruzzini, M.; Sessoli, R. *Inorg. Chem.* **2012**, *51*, 6962−6968.
(10) Wang, Z. M.; Hu, K. L.; Gao, S.; Kobayashi, H. *Adv. Mater.* **2010**, *22*, 1526−1533.
(11) Hu, K. L.; Kurmoo, M.; Wang, Z. M.; Gao, S. *Chem.—Eur. J.* **2009**, *15*, 12050−12064.
(12) Wang, Z. M.; Zhang, X. Y.; Batten, S. R.; Kurmoo, M.; Gao, S. *Inorg. Chem.* **2007**, *46*, 8439−8441.
(13) Duan, Z.; Wang, Z.; Gao, S. *Dalton Trans.* **2011**, *40*, 4465−4473.
(14) Paredes-García, V.; Vega, A.; Novak, M. A.; Vaz, M. G. F.; Souza, D. A.; Venegas-Yazigi, D.; Spodine, E. *Inorg. Chem.* **2009**, *48*, 4737−4742.
(15) Zeng, M.-H.; Wang, B.; Wang, X.-Y.; Zhang, W.-X.; Chen, X.-M.; Gao, S. *Inorg. Chem.* **2006**, *45*, 7069−7076.
(16) Barron, L. D. *Nat. Mater.* **2008**, *7*, 691−692.
(17) Golobič, A.; Malekovič, M.; Šegedin, P. *Acta Crystallogr.* **2006**, *C62*, m102−m104.
(18) Bruker (2007). *SAINT*. Bruker AXS Inc.: Wisconsin, USA.
(19) Bruker (2001). *SADABS*. Bruker AXS Inc.: Wisconsin, USA.
(20) Oxford Diffraction (2006). *CrysAlis Pro;* Oxford Diffraction Ltd: England.
(21) Sheldrick, G. *Acta Crystallogr.* **2008**, *A64*, 112−122.
(22) Dolomanov, O. V.; Bourhis, L. J.; Gildea, R. J.; Howard, J. A. K.; Puschmann, H. *J. Appl. Crystallogr.* **2009**, *42*, 339−341.
(23) Farrugia, L. *J. Appl. Crystallogr.* **1999**, *32*, 837−838.
(24) Kato, K.; Hirose, R.; Takemoto, M.; Ha, S.; Kim, J.; Higuchi, M.; Matsuda, R.; Kitagawa, S.; Takata, M. *AIP Conf. Proc.* **2010**, *1234*, 875−878.
(25) Rodríguez-Carvajal, J. *Phys. B* **1993**, *192*, 55−69.
(26) Wolff, S. K.; Grimwood, D. J.; McKinnon, J. J.; Turner, M. J.; Jayatilaka, D.; Spackman, M. A. *CrystalExplorer,* Version 3.0; University of Western Australia, 2012.
(27) Bergerhoff, G.; Brown, I. D. In *Crystallographic Databases;* Allen, F. H. (Hrsg.): Chester, England, 1987.
(28) Bain, G. A.; Berry, J. F. *J. Chem. Educ.* **2008**, *85*, 532−536.
(29) Grohol, D.; Matan, K.; Cho, J.-H.; Lee, S.-H.; Lynn, J. W.; Nocera, D. G.; Lee, Y. S. *Nat. Mater.* **2005**, *4*, 323−328.
(30) Agterberg, F. P. W.; Provó Kluit, H. A. J.; Driessen, W. L.; Reedijk, J.; Oevering, H.; Buijs, W.; Veldman, N.; Lakin, M. T.; Spek, A. L. *Inorg. Chim. Acta* **1998**, *267*, 183−192.
(31) Tranchemontagne, D. J.; Mendoza-Cortés, J. L.; O'Keeffe, M.; Yaghi, O. M. *Chem. Soc. Rev.* **2009**, *38*, 1257−1283.
(32) Turner, M. J.; McKinnon, J. J.; Jayatilaka, D.; Spackman, M. A. *CrystEngComm* **2011**, *13*, 1804−1813.
(33) Filsø, M. Ø.; Turner, M. J.; Gibbs, G. V.; Adams, S.; Spackman, M. A.; Iversen, B. B. *Chem.—Eur. J.* **2013**, *19*, 15535−15544.
(34) Jayalakshmi, M.; Scholz, F. *J. Power Sources* **2000**, *91*, 217−223.
(35) Yabuuchi, N.; Kajiyama, M.; Iwatate, J.; Nishikawa, H.; Hitomi, S.; Okuyama, R.; Usui, R.; Yamada, Y.; Komaba, S. *Nat. Mater.* **2012**, *11*, 512−517.
(36) Masquelier, C.; d'Yvoire, F.; Bretey, E.; Berthet, P.; Peytour-Chansac, C. *Solid State Ionics* **1994**, *67*, 183−189.
(37) Park, Y.-U.; Seo, D.-H.; Kwon, H.-S.; Kim, B.; Kim, J.; Kim, H.; Kim, I.; Yoo, H.-I.; Kang, K. *J. Am. Chem. Soc.* **2013**, *135*, 13870−13878.
(38) West, A. R. *In Basic Solid State Chemistry,* 2nd ed.; John Wiley & Sons, Ltd, 1999; pp 377−380.
(39) Zhang, B.; Wang, Z.; Kurmoo, M.; Gao, S.; Inoue, K.; Kobayashi, H. *Adv. Funct. Mater.* **2007**, *17*, 577−584.